

# Multi-line lasing in the broadly tunable ammonia quantum cascade laser pumped molecular laser

Paul Chevalier, Arman Amirzhan, and Federico Capasso

*Harvard John A. Paulson School of Engineering and Applied Sciences,*

*Harvard University, Cambridge, MA 02138, USA*

Jeremy Rowlette, H. Ted Stinson, Michael Pushkarsky, and Timothy Day

*DRS Daylight Solutions, San Diego, CA 92128*

Henry O. Everitt

*DEVCOM Army Research Lab, Houston, TX 77005 and*

*Department of Physics, Duke University, Durham, NC 27708, USA*

([\\*capasso@seas.harvard.edu](mailto:capasso@seas.harvard.edu), [everitt@phy.duke.edu](mailto:everitt@phy.duke.edu))

## Abstract

Gaseous ammonia has previously been demonstrated as a compelling gain medium for a quantum cascade laser pumped molecular laser (QPML), exhibiting good power efficiency but limited tunability. Here we explore the potential of the ammonia QPML to produce powerful, broadly tunable terahertz frequency lasing on rotational and pure inversion transitions. After theoretically predicting possible laser frequencies, pump thresholds, and efficiencies, we experimentally demonstrate unprecedented tunability – from 0.762 to more than 4.5 THz – by pumping Q- and R-branch infrared transitions with widely tunable quantum cascade lasers. We additionally demonstrate two types of multi-line lasing: simultaneous pure inversion and rotation-inversion transitions from the same pumped rotational state, and cascaded lasing involving transitions below the pumped rotational state. We report single frequency power levels as great as 0.33 mW from a low volume laser cavity.

The quest for powerful, tunable, continuous wave sources of terahertz radiation for use in spectroscopy, communications, imaging, and radar has recently been accelerated by the development of a new type of source: a quantum cascade laser-pumped molecular laser (QPML).[1–3] A molecular gas in a compact laser cavity can be made to lase on any rotational transition of virtually any molecule that has a permanent electric dipole moment, a vapor pressure, and an infrared (IR) rotational-vibrational absorption band that may be spanned by a tunable quantum cascade laser (QCL). By tuning the QCL frequency to coincide with any such ro-vibrational transition  $J_L \rightarrow J_U$ , it has been previously shown that two rotational population inversions may be created, the direct transition between  $J_U \rightarrow J_U - 1$  of the excited vibrational level and the refilling transition between  $J_L + 1 \rightarrow J_L$  of the ground vibrational level. [1, 4] The length of the cavity containing the gas may then be adjusted so one of its resonant frequencies coincides with one or the other of these transitions. Thus, a single molecular gain medium may be made to lase simply by tuning both the QCL to a specific IR frequency and the QPML cavity to the terahertz frequency of the transition. In this manner, any molecular rotational absorption transition may be made to lase, and millions of such transition frequencies have been measured or tabulated.[5–7]

Ammonia was the first molecule made to lase in this manner, [2] although not on rotational transitions but on widely-spaced pure inversion transitions in the  $v_2 = 1$  excited vibrational band (corresponding the molecule's wagging mode). The pure inversion transition frequencies in  $v_2 = 1$  are much larger than the well-known ground state microwave transitions (9-35 GHz) because the inversion energy is comparable to the height of the tunnel barrier. Consequently, the inversion splittings in  $v_2 = 1$  are strong transitions clustered near 1.1 THz. A handful of such pure inversion laser transitions have been reported, including one that yielded 1 mW of output power, when a Q-branch ( $J_L = J_U = J$ ) transition was pumped by a narrowly tunable QCL operating between 965-968 cm<sup>-1</sup>. [3] More recently, rotation-inversion transitions pumped by R-branch IR transitions in <sup>15</sup>NH<sub>3</sub> were made to lase around 4.5 THz. [8]

By using a widely tunable pump source, we have demonstrated that the simple linear molecule nitrous oxide (N<sub>2</sub>O) can achieve continuous-wave laser emission for at least 39 transitions with discrete line tunability from 0.25 to 0.95 THz. [1] More recently we demonstrated that using a prolate symmetric top molecule (methyl fluoride or CH<sub>3</sub>F) as the gain medium allows for an unprecedented tunability with emission on 120 lines spanning from 0.3 GHz up to 1.3 THz. [9]

In this letter, we demonstrate the broad tunability that is possible from the ammonia QPML when rotation-inversion transitions are made to lase. We have discovered and characterized two

multi-line lasing mechanisms in the ammonia QPML: the simultaneous lasing of a pure inversion and a rotation-inversion transition sharing the same pumped upper level, and the cascaded lasing from a lower energy lasing transition indirectly connected to the pumped level. Both mechanisms allow simultaneous lasing at two very different frequencies, and in certain cases the cascade mechanism allows for lasing at frequencies that would not be directly possible due to the selection rules.

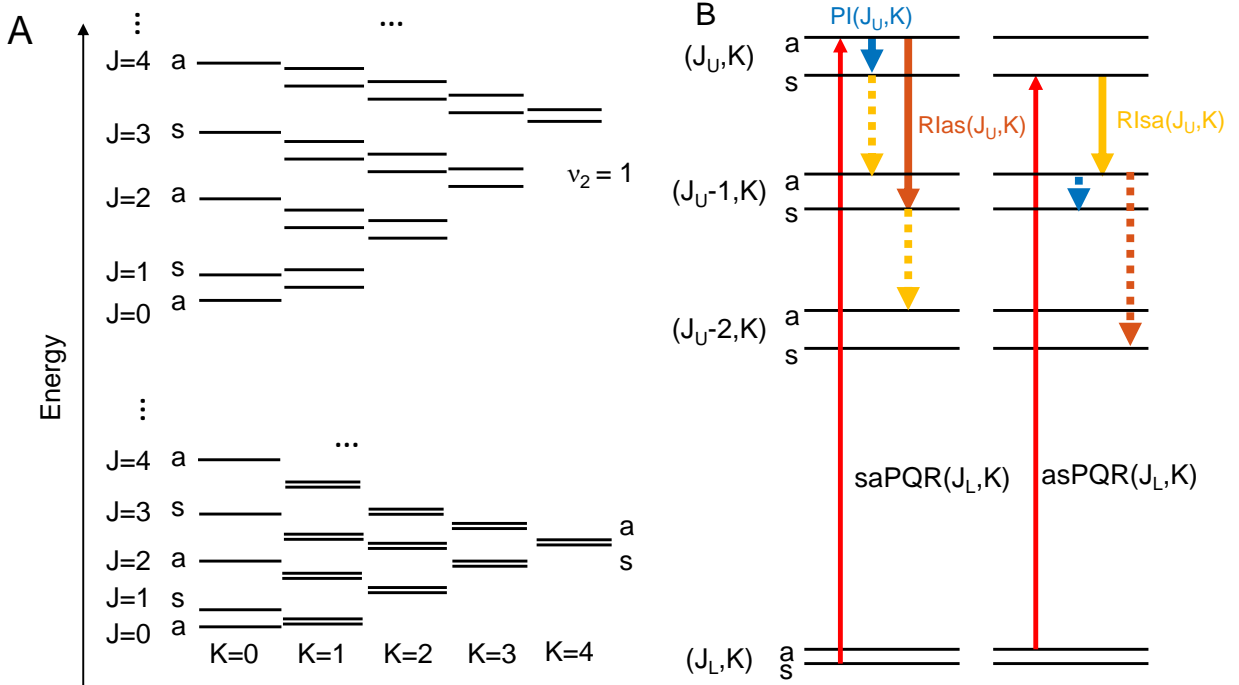


FIG. 1. (A) Energy level diagram of  $\text{NH}_3$  in the ground and  $v_2 = 1$  vibrational states. Note the alternating s and a levels at  $K = 0$ . (B) Three types of laser transitions are possible in  $\text{NH}_3$  QPMLs: pure inversion (PI, blue) and rotation-inversion (RIas, red) when an  $s \rightarrow a$  IR transition is pumped, and rotation-inversion (RIsa, yellow) for an  $a \rightarrow s$  IR pump. Cascaded transitions for each type are illustrated as dashed arrows of the same colors.

It is well known that ammonia's rotational spectrum is complicated by the inversion splitting caused by the inversion tunneling of the nitrogen atom in this pyramidal molecule[10, 11]. A simplified version of the energy level diagram for the ammonia molecule for  $J \leq 3$  is given in Fig. 1(A). Whether for pumping or lasing, the selection rules require a change in symmetry of the two energy levels associated with the inversion doublet, symmetric (s) and anti-symmetric (a), so the only allowed transitions are  $a \rightarrow s$  or  $s \rightarrow a$ . Consequently, pure inversion transitions and Q-branch transitions ( $\Delta J = 0$ ) with  $K = 0$  are forbidden. Because  $\text{NH}_3$  is an oblate symmetric top,

the lowest energy levels occur for  $J = K$ , and these are generally the most heavily populated.

Because of the inversion splitting, two types of IR – P, Q, or R branch – transitions may pump population into a given rotational state  $(J, K)$  (see Fig. 1(B))), where the  $J$  is the quantum number representing the total angular momentum, and  $K$  represents the projection of the angular momentum along the symmetry axis of the molecule. The first is a higher energy transition connecting a lower symmetric inversion level in the ground vibrational state to a higher antisymmetric inversion level in  $v_2 = 1$ , denoted  $saP(J, K)$ ,  $saQ(J, K)$ , or  $saR(J, K)$ , respectively spanning 679-948, 954-968, or 1007-1249  $\text{cm}^{-1}$  for  $J \leq 14$ . The converse transitions  $asP(J, K)$ ,  $asQ(J, K)$ , and  $asR(J, K)$  occur at lower frequencies for a given  $J$  (respectively 632-932, 905-949, or 952-1237  $\text{cm}^{-1}$  for  $0 \leq J \leq 14$ ).

When an  $saQ(J, K)$  transition is pumped, two QPML direct lasing transitions may occur (shown on the left side of Fig. 1(B)): the pure inversion transition  $(J, K, a) \rightarrow (J, K, s)$  and the rotation-inversion transition  $(J, K, a) \rightarrow (J - 1, K, s)$ . Symmetry-based selection rules only allow the  $sa$  pump transitions to produce lasing on pure inversion transitions. When an  $asQ(J, K)$  transition is pumped, the rotation-inversion transition  $(J, K, s) \rightarrow (J - 1, K, a)$  may be made to lase (right side of Fig. 1(B)). For simplicity, we label these three QPML transitions in  $v_2 = 1$  as  $PI(J, K)$ ,  $RIas(J, K)$ , and  $RIsa(J, K)$ , respectively. Similarly, pumping an R( $J, K$ ) or P( $J, K$ ) transition may induce lasing on transitions with  $J_U = J + 1$  or  $J_U = J - 1$ , respectively. To date, ammonia QPMLs have been demonstrated either lasing on PI lines pumped by Q-branch transitions, [2, 3] or on RIas lines pumped by R-branch transitions. [8] In the following, we consider all three types of lasing transitions from Q or R branch pump transitions, both  $s \rightarrow a$  and  $a \rightarrow s$ .

To explore the relative tunability and efficacy of all three types of transitions systematically, we use the the same method as described in our previous work [9] to compute the normalized slope efficiency and lasing threshold power for direct PI and RI lasing transitions of the ammonia laser. The first step is to compute the energy levels of ammonia as a function of  $J$ ,  $K$ , and inversion state (a or s) using the published rotational constants for ammonia [12–14]. From these energy levels and the selection rules mentioned above, one can compute the expected direct lasing frequencies as a function of the pump wavenumber for Q and R-branch IR transitions. Representative transitions for those lines with  $K$  a multiple of 3, plotted respectively in Figs. 2(A) and 2(B), reveal that ammonia can be used as a gain medium in a widely tunable QPML spanning the frequency range 0.140 – 9.634 THz, far beyond the limited tunability afforded by PI transitions clustered at  $1.1 \pm 0.3$  THz.

For threshold, slope efficiency, and power, one must compute the population fraction for each

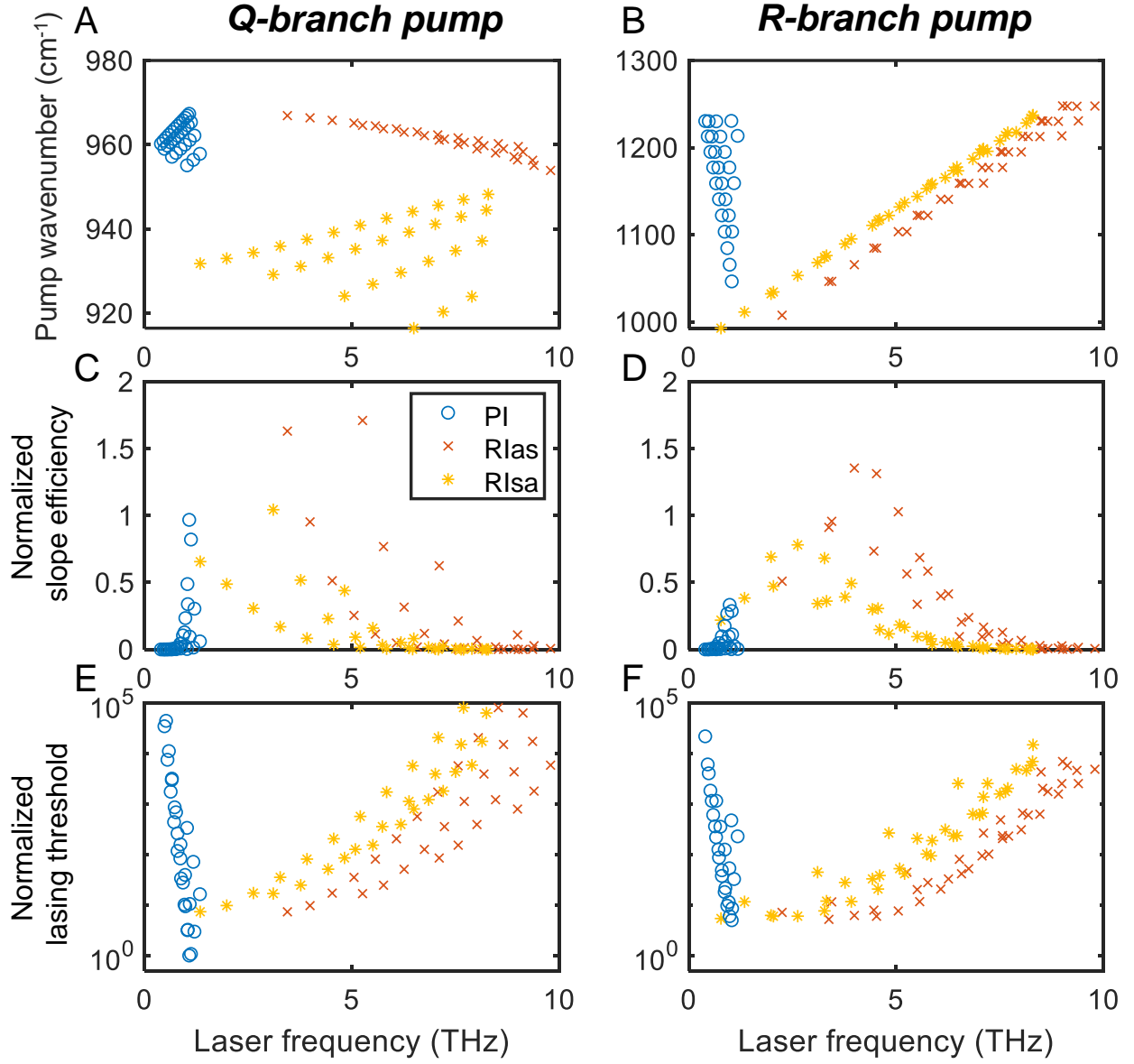


FIG. 2. Direct lasing transition frequencies for the  $\text{NH}_3$  QPML, plotting only those transitions with  $K$  multiple of 3 for (A) a Q-branch or (B) an R-branch pump. Normalized slope efficiency (C,D) and threshold (E,F) of the  $\text{NH}_3$  QPML for those transitions, using the method of Ref. 9 for (C,E) a Q-branch or (D,F) an R-branch pump.

energy level and branching ratios for each transition as a function of  $J$ ,  $K$ , and inversion state for all Q or R pumped transitions and the corresponding PI, RIas, and RIasa lasing transitions. [10] The Q-branch and pure inversion transitions are governed by a branching ratio that goes as  $K^2$ , while the R-branch and rotation-inversion transitions are governed by branching ratios that go as  $(J + 1)^2 -$

$K^2$  or  $J^2 - K^2$ , respectively. Thus, Q-branch and pure inversion transitions are favored for large  $K$  while R-branch and rotation-inversion transitions are favored for small  $K$ . Figures 2(C) and 2(E) respectively give the normalized slope efficiency and lasing threshold for Q-branch pumped lasing transitions with  $K$  multiple of 3. Similar plots are shown in Figs. 2(D) and 2(F) for an R-branch pump. The slope efficiencies and lasing thresholds have been normalized by the values for the lowest threshold lasing line (Q branch pumped pure inversion,  $J = 4, K = 3$ ) in order to simplify line-by-line comparisons, since the absolute number strongly depends on cavity geometry and loss. Complete plots for all values of  $K$  are given in the supplementary document, along with a table giving all the calculated transition frequencies for  $J_L \leq 10$ .

To verify these predictions, we used the experimental setup depicted in Fig. 3(A). IR light from an external cavity (EC)-QCL (Daylight Solutions 41095-HHG-UT, tunable from 920 to 1194  $\text{cm}^{-1}$ ) is injected through a Brewster's angle ZnSe window into a THz cavity that consists of a 50 cm long copper pipe with a 4.8 mm internal diameter. A flat mirror with a centered 1 mm diameter pinhole is used as an output coupler. The cavity resonance frequency was tuned by changing the tuning mirror position to adjust the cavity length. Compared to the previous demonstration of the methyl fluoride QPML, the rear mirror of the cavity can either be a flat mirror, or a pinhole coupler (pinhole diameter 1.7 mm) sealed by a 4 mm thick polymethylpentene (TPX) window. Light from the rear of the cavity can be characterized by a Tydex TSFPI-2 scanning Fabry-Perot interferometer (SFPI) coupled with a broadband THz detector (Golay cell): where the periodicity of interference fringes as a function of the path difference corresponds to the half-wavelength of the emitted light. The front ZnSe coupler absorbs light at frequencies above 2 THz, thereby acting as a low pass terahertz filter, while the TPX rear window transmits all terahertz frequencies. Outgoing terahertz light generated in the laser cavity can either be collected from the front of the laser by an off-axis parabolic mirror and focused onto a detector using a 75 mm focal length TPX lens, or directly collected from the rear pinhole coupler. A separate gas absorption cell containing 100 mTorr of anhydrous ammonia was used to monitor how precisely the QCL emission frequency was tuned to the desired  $\text{NH}_3$  roto-vibrational transition.

To begin, we pumped the QPML cell containing 20 mTorr of ammonia with the widely tunable QCL and measured 24 direct PI and RI lasing transitions spanning 0.769-4.46 THz by tuning the QCL across Q- and R-branch transitions from 966.27-967.41 and 992.70-1084.72  $\text{cm}^{-1}$ . As can be seen in Fig. 1(B), either a pure inversion (blue solid arrow) or a rotation-inversion (red solid arrow) transition may be made to lase. Surprisingly, when we pumped the saR(4, 3) IR transition

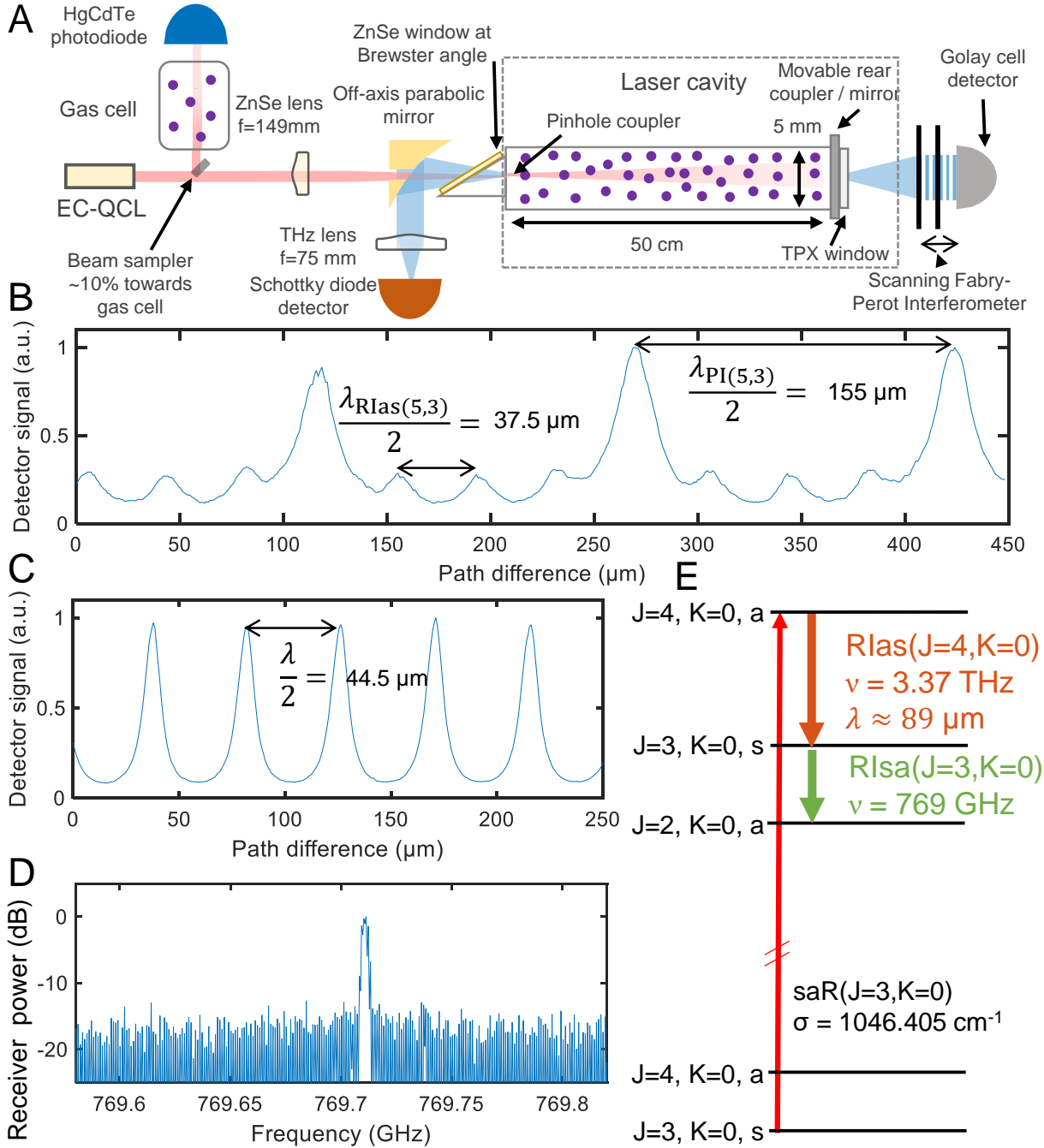


FIG. 3. (A) Experimental schematic of the  $\text{NH}_3$  QPML: the 4.8 mm diameter, 50 cm long copper laser cavity has pinhole output couplers in the front and rear. (B) Interferogram measured with a scanning Fabry Perot inteferometer (SFPI), showing simultaneous lasing at 0.97 THz and 3.97 THz (wavelengths 310  $\mu\text{m}$  and 75  $\mu\text{m}$ ). (C) Measured interferogram showing a laser emission frequency of 3.37 THz (89  $\mu\text{m}$  wavelength). (D) Signal measured with a receiving mixer showing laser emission at 769 GHz. (E) Mechanism for simultaneous direct and cascaded laser emission in a  $\text{NH}_3$  QPML pumped by the asR(3,0) IR transition.

at  $1065.57\text{ cm}^{-1}$ , we observed both PI and RI lines to lase simultaneously. Figure 3(B), which plots the measured signal on the Golay cell as a function of the path difference of the SFPI, exhibits two periodicities corresponding to simultaneous emission near  $0.97\text{ THz}$  ( $\text{PI}(5,3)$ ) and  $3.97\text{ THz}$  ( $\text{RIas}(5,3)$ ). Without a spectrometer to discriminate these two lines the total power emitted could have been mistakenly ascribed to just one of them. Experimentally, the relative magnitude of each line can be adjusted by changing the cavity length and thereby tuning the cavity resonance to match either frequency.

We then pumped the same cell with the QCL tuned to the  $\text{saR}(3,0)$  IR transition ( $1046.405\text{ cm}^{-1}$ ), since the Q-branch version of this transition is forbidden. The pure inversion lasing transition is forbidden for  $K = 0$  because the  $(4,0,\text{s})$  and  $(3,0,\text{a})$  levels do not exist. The QPML was made to lase on the RI transition, and light at  $3.37\text{ THz}$  was measured from the rear output coupler (solid red arrow in Fig. 1(B) for reference. The emission frequency was determined by the SFPI, using the measured interferogram shown in Fig. 3(C).

Surprisingly, light was also measured from the front output coupler at  $769\text{ GHz}$ , using a receiving mixer (VDI SAX WR1.0), as shown in Fig. 3(C). According to the selection rules and calculated energy levels, [12, 13] only direct lasing at  $3.37\text{ THz}$  should be expected. The presence of light at two significantly different frequencies for the  $\text{saR}(3,0)$  pump transition can be explained by the energy diagrams in Figs. 1(B) (yellow dashed arrow below solid red arrow) and 3(D). Molecules that mediated the laser emission at  $3.37\text{ THz}$  ( $\text{RIas}(4,0)$ ) have relaxed to  $(3,0,\text{s})$ . At low gas pressures where collisional relaxation is very slow, these molecules in  $(3,0,\text{s})$  created another population inversion above  $(2,0,\text{a})$ . This second population inversion can then emit light at the  $\text{RIsa}(3,0)$  frequency once it reaches the lasing threshold, which is what was observed.

Unlike the situation shown in Fig. 3(B), the SFPI interferogram in Fig. 3(C) does not exhibit a second periodicity at half the wavelength of the cascaded line ( $195\text{ }\mu\text{m}$ ). This shows that the power emitted at the cascaded line is much lower than at the direct frequency. Using a calibrated calorimeter detector (VDI PM5B) we measured a total output power of  $0.33\text{ mW}$  in this configuration. Because of its magnitude, we can attribute at least 95% of this output power to the direct line lasing at  $3.37\text{ THz}$ .

In order to confirm cascaded lasing, we measured the detected signal at  $769\text{ GHz}$  as a function of the pump power and ammonia pressure for both the direct RI transition (pumped by  $\text{asR}(2,0)$  at  $992.70\text{ cm}^{-1}$ ) and the cascaded line (pumped by  $\text{saR}(3,0)$ ), and the result is plotted in Figs. 4(A) and 4(C) respectively. These measurements were both conducted using a flat mirror instead of a

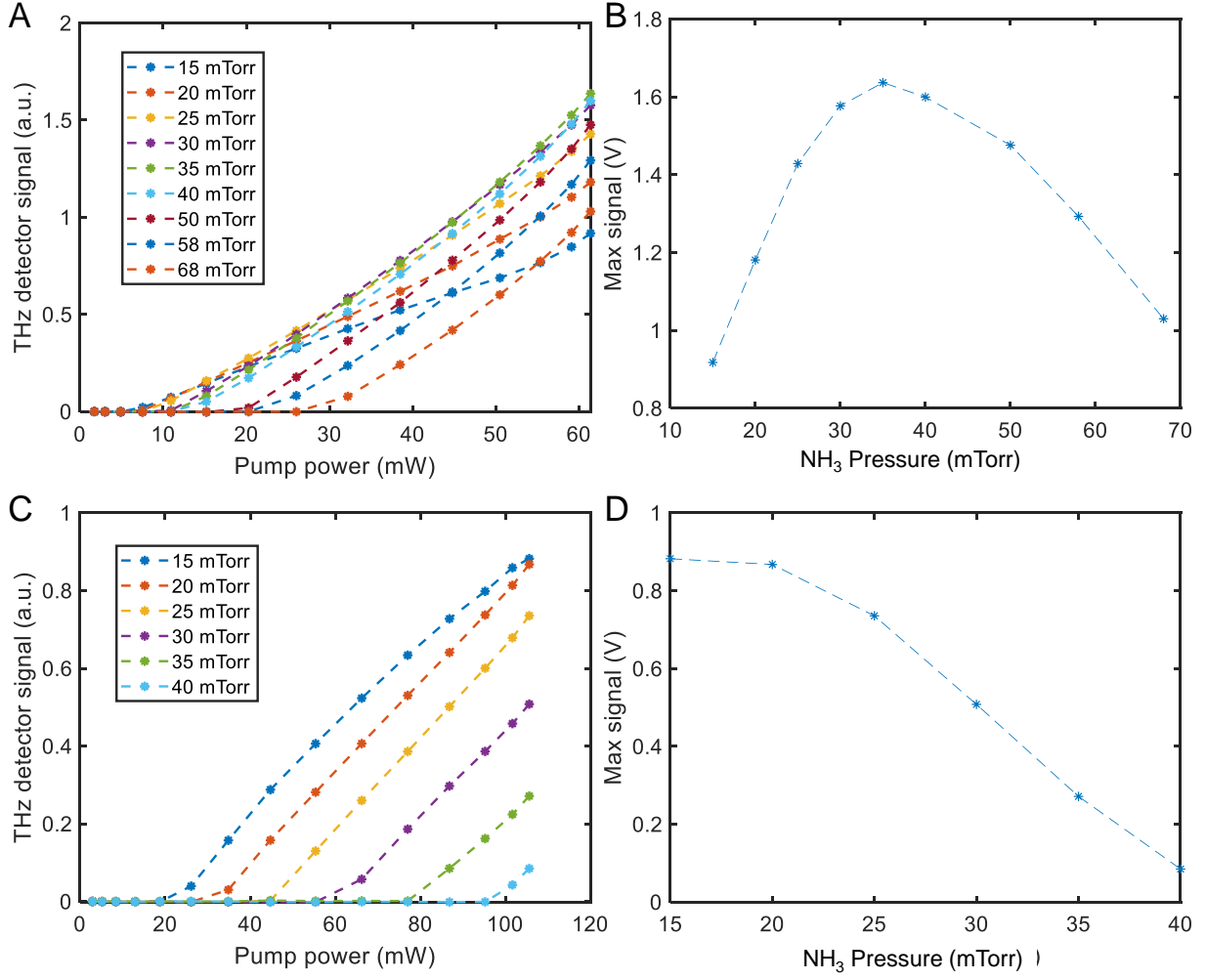


FIG. 4. (A) Plot of the detected signal at 769 GHz for an infrared pump at  $992.70\text{ cm}^{-1}$  (direct lasing line) as a function of the pump power and gas pressure. (B) Plot of the peak signal from (A) as a function of the gas pressure. (C) Plot of the detector signal at 769 GHz for an infrared pump at  $1046.405\text{ cm}^{-1}$  (cascaded lasing line) as a function of the pump power and gas pressure. (D) Plot of the peak signal from (C) as a function of the gas pressure.

pinhole coupler at the rear of the cavity in order to lower the radiative cavity losses. Notice that the cascaded lasing threshold is higher than the direct lasing threshold, an indication of a different excitation mechanism. Additionally the peak signal measured at the maximum available pump power for the respective pump frequencies (89 mW at  $992.70\text{ cm}^{-1}$  and 152 mW at  $1046.405\text{ cm}^{-1}$ ) is plotted as a function of the gas pressure in the cell in Figs. 4(B) and 4(D). As further confirmation of the differing excitation mechanisms, notice that the cascaded lasing is more effi-

TABLE I. Table giving the frequency of measured cascaded lines along with their direct pump wavenumber.

Frequency (GHz)	Transition type	Direct R pump wavenumber (cm <sup>-1</sup> )	Cascaded R pump wavenumber (cm <sup>-1</sup> )	Direct Q pump wavenumber (cm <sup>-1</sup> )
769	RI <sub>a</sub> (3,0)	asR(2,0) @ 992.70	saR(3,0) @ 1046.405	not allowed
762	RI <sub>a</sub> (3,1)	asR(2,1) @ 992.45	saR(3,1) @ 1046.4 or saR(2,1) @ 1027.047	asQ(3,1) @ 967.45
1393	RI <sub>a</sub> (4,1)	asR(3,1) @ 1013.17	saR(4,1) @ 1065.59 or saR(3,1) @ 1046.40	asQ(4,1) @ 967.03
1073	PI(3,3)	not allowed	asR(3,3) @ 1011.20	asQ(3,3) @ 967.34
1035	PI(4,3)	saR(3,3) @ 1046.37	asR(4,3) @ 1032.13	asQ(4,3) @ 966.90
979.6	PI(5,3)	saR(4,3) @ 1065.56	asR(5,3) @ 1053.13	asQ(5,3) @ 966.38

cient at low pressure, reaching maximum power at 15 mTorr, while direct lasing is more efficient at higher pressure, reaching maximum power at 30 mTorr.

This *cascaded* lasing, as opposed to *direct* lasing, has been seen on a few transitions in other optically pumped far-IR laser gases at low pressures and high pump powers.[15] However, with tunable QCLs this cascaded lasing at low pressure is possible on most transitions in most molecules, including ammonia. As summarized in Table I, we observed cascaded lasing on six lines, including lines for which  $K \neq 0$  and PI transitions are also allowed. For example, we observed cascaded lasing when pumping saR(3,1), with laser emission measured at 762 GHz and corresponding to the RI<sub>a</sub>(3,1) line. By appropriately tuning the cavity resonance we measured laser emission on the PI( $J = 4, K = 1$ ) when pumping the same saR( $J = 3, K = 1$ ) IR transition. The threshold of the PI line was qualitatively larger than the one of the cascaded transition. In general, the choice of the  $K$  value is particularly important to determine which type of cascaded line can be made to lase. As noted above, pure inversion transitions are favored for large  $K$  while rotation-inversion transitions are favored for small  $K$ . Thus, by choosing  $K$  close to 0, the threshold of any pure inversion line is significantly increased, and cascaded lasing is more likely to happen on a rotation inversion line. Conversely, by choosing  $K$  close to  $J$ , PI transitions will have a lower lasing threshold are will be more likely to be measured as cascaded transitions.

From these observations is has become apparent that two types of simultaneous multi-line lasing transitions, multiple direct and cascaded, exist in ammonia. Specifically, the saPQR( $J_L, K$ )

pump can generate simultaneous lasing on two direct transitions,  $\text{PI}(J_U, K)$  and  $\text{RIas}(J_U, K)$ , each of which can produce lasing on a different cascaded laser transition,  $\text{RIsa}(J_U, K)$  and  $\text{RIsa}(J_{U-1}, K)$  respectively. By contrast, the  $\text{asPQR}(J_L, K)$  pump can create only one direct transition,  $\text{RIas}(J_U, K)$ , but it can produce two cascaded lasing transitions,  $\text{PI}(J_{U-1}, K)$  and  $\text{RIas}(J_{U-1}, K)$ . In either case, which lines actually lase is determined by the transition-unique branching ratios, energy levels, and cavity tuning, but it is possible that up to four or three lines of significantly different frequency may lase simultaneously in the former or latter cases, respectively. This multi-line lasing attribute adds further excitement to the ammonia QPML, whose unique energy level spectrum already permits broad single line tunability from 0.140 to 9.634 THz.

## ACKNOWLEDGMENTS

The authors acknowledge S. Cotreau and A. DiMambro of Harvard University Instructional machine shop for their help with fabrication of the THz cavity elements. This work was partially supported by the U.S. Army Research Office (contracts W911NF-19-2-0168, W911NF-20-1-0157) and DRS Daylight Solutions. Any opinions, findings, conclusions, or recommendations expressed in this material are those of the authors and do not necessarily reflect the views of the Assistant Secretary of Defense for Research.

## DATA AVAILABILITY STATEMENT

The data that support the findings of this study are available from the corresponding author upon reasonable request.

## REFERENCES

---

- [1] P. Chevalier, A. Amirzhan, F. Wang, M. Piccardo, S. G. Johnson, F. Capasso, and H. O. Everitt, *Science* **366**, 856 (2019).
- [2] A. Pagies, G. Ducournau, and J.-F. Lampin, *APL Photonics* **1**, 031302 (2016).

- [3] J.-F. Lampin, A. Pagies, G. Santarelli, J. Hesler, W. Hansel, R. Holzwarth, and S. Barbieri, *Optics Express* **28**, 2091 (2020).
- [4] F. Wang, J. Lee, D. J. Phillips, S. G. Holliday, S.-L. Chua, J. Bravo-Abad, J. D. Joannopoulos, M. Soljačić, S. G. Johnson, and H. O. Everitt, *Proceedings of the National Academy of Sciences* **115**, 6614 (2018).
- [5] *JPL Molecular Spectroscopy Database* (2017).
- [6] *Splatatalogue Database for Astronomical Spectroscopy* (2007).
- [7] R. Kochanov, I. Gordon, L. Rothman, K. Shine, S. Sharpe, T. Johnson, T. Wallington, J. Harrison, P. Bernath, M. Birk, G. Wagner, K. L. Bris, I. Bravo, and C. Hill, *Journal of Quantitative Spectroscopy and Radiative Transfer* (2019), 10.1016/j.jqsrt.2019.04.001.
- [8] M. Wienold, A. Zubairova, and H.-W. Hübers, *Optics Express* **28**, 23114 (2020).
- [9] A. Amirzhan, P. Chevalier, J. Rowlette, H. T. Stinson, M. Pushkarsky, T. Day, H. O. Everitt, and F. Capasso, arXiv preprint arXiv:2105.13326 (2021).
- [10] W. Gordy, R. L. Cook, and A. Weissberger, *Microwave molecular spectra*, Vol. 18 (Wiley New York, 1984).
- [11] C. H. Townes and A. L. Schawlow, *Microwave spectroscopy* (Dover Publications, 1975).
- [12] R. Poynter and J. Margolis, *Molecular Physics* **48**, 401 (1983).
- [13] R. Poynter and J. Margolis, *Molecular Physics* **51**, 393 (1984).
- [14] H. Mould, W. Price, and G. Wilkinson, *Spectrochimica Acta* **15**, 313 (1959).
- [15] K. J. Button, *Reviews of Infrared and Millimeter Waves: Volume 2 Optically Pumped Far-Infrared Lasers* (Springer Science & Business Media, 2013).

## Supplementary document: Multi-line lasing in the broadly tunable ammonia quantum cascade laser pumped molecular laser

Paul Chevalier, Arman Amirzhan, and Federico Capasso

*Harvard John A. Paulson School of Engineering and Applied Sciences, Harvard University, Cambridge, MA 02138, USA*

Jeremy Rowlette, H. Ted Stinson, Michael Pushkarsky, and Timothy Day  
*DRS Daylight Solutions, San Diego, CA 92128*

Henry O. Everitt

*DEVCOM Army Research Lab, Houston, TX 77005 and  
 Department of Physics, Duke University, Durham, NC 27708, USA  
 (\*capasso@seas.harvard.edu,everitt@phy.duke.edu)*

This document contains additional tables and figures to support the content of the main text.

Figure 1 recalls the labels for direct and cascaded lasing transition in ammonia QPMLs. Figures 2-4 along with the numbers in Table I-IV were obtained using published rota-

tional constants of the ammonia molecule[1-3]. The method to obtain the lasing frequencies, normalized threshold and normalized slope efficiency from the rotational constants is given in Ref. 4.

[1] R. Poynter and J. Margolis, *Molecular Physics* **48**, 401 (1983).  
 [2] R. Poynter and J. Margolis, *Molecular Physics* **51**, 393 (1984).  
 [3] H. Mould, W. Price, and G. Wilkinson, *Spectrochimica Acta* **15**, 313 (1959).

[4] A. Amirzhan, P. Chevalier, J. Rowlette, H. T. Stinson, M. Pushkarsky, T. Day, H. O. Everitt, and F. Capasso, arXiv preprint arXiv:2105.13326 (2021).

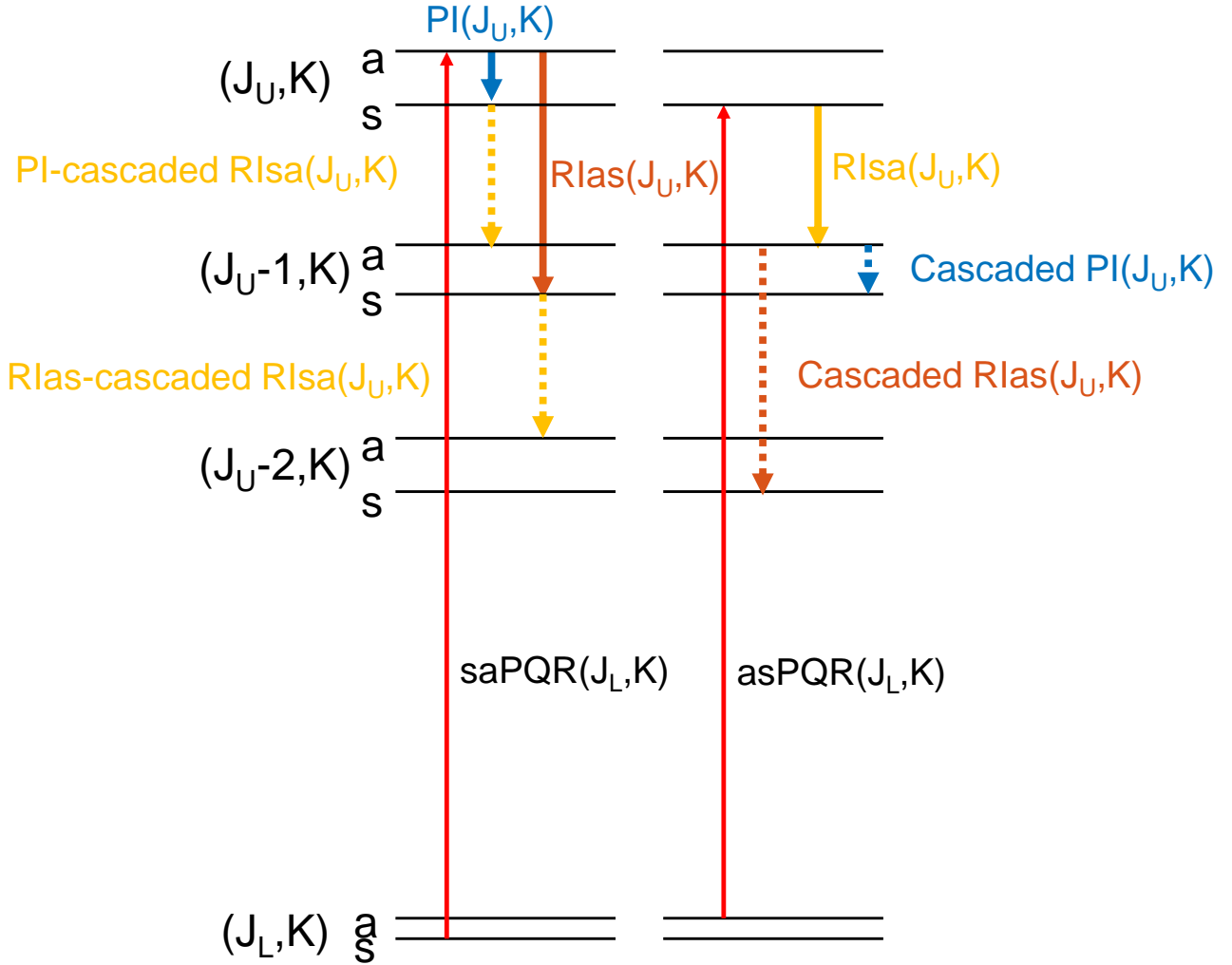


FIG. 1. Three types of laser transitions are possible in  $\text{NH}_3$  QPMLs: pure inversion (PI, blue) and rotation-inversion (RIas, red) when an  $s \rightarrow a$  IR transition is pumped, and rotation-inversion (RIsa, yellow) for an  $a \rightarrow s$  IR pump. Cascaded transitions for each type are illustrated as dashed arrows of the same colors. When an  $sa$  pump is used, two type of cascaded transitions can occur: a PI-cascaded RIsa and an asRI-cascaded RIsa. When an  $as$  pump is used two type of cascaded transitions can occur: a cascaded PI transition or a cascaded RIas transition.

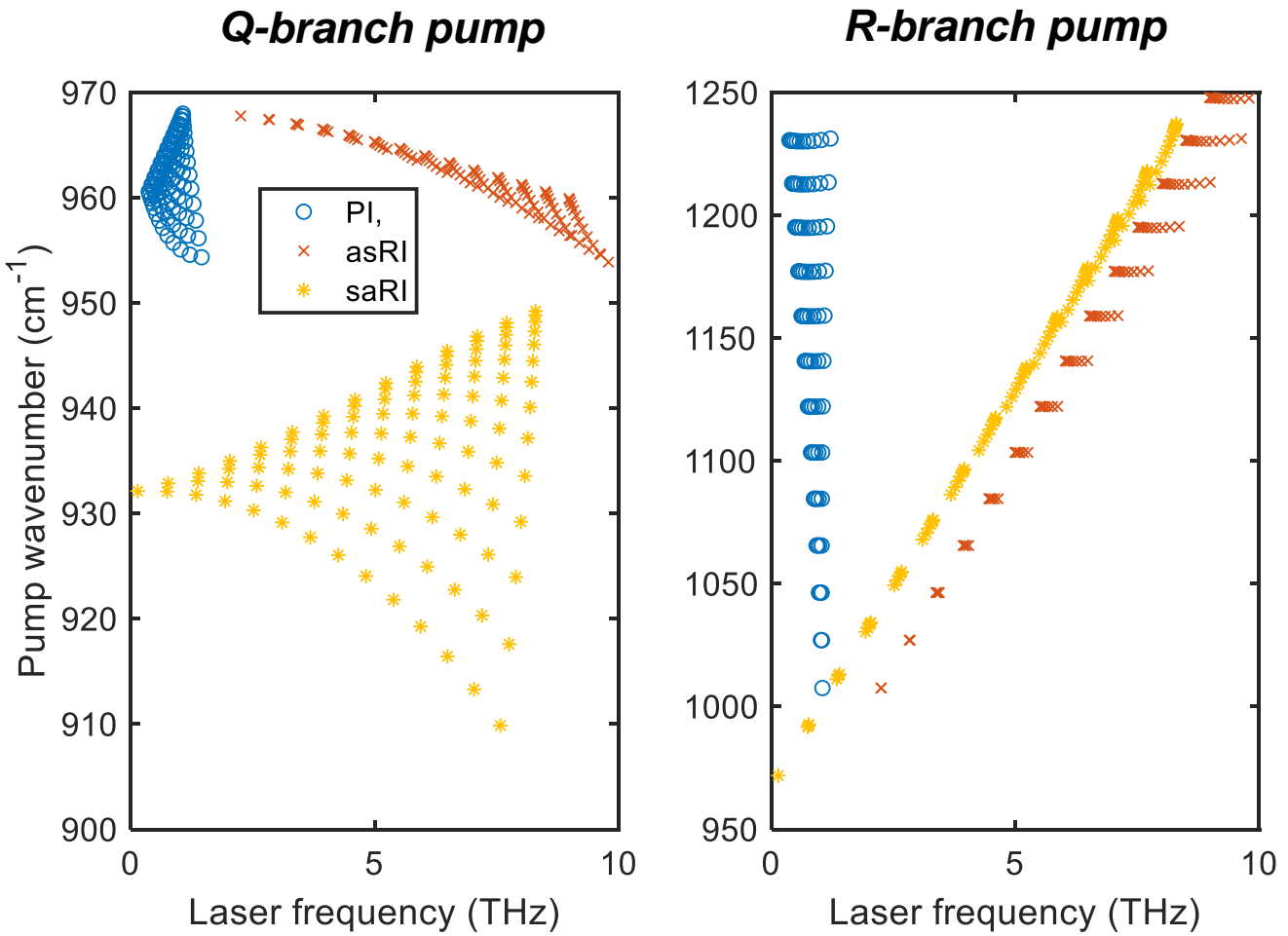


FIG. 2. Direct lasing transition frequencies for the  $\text{NH}_3$  QPML a Q-branch or an R-branch pump.

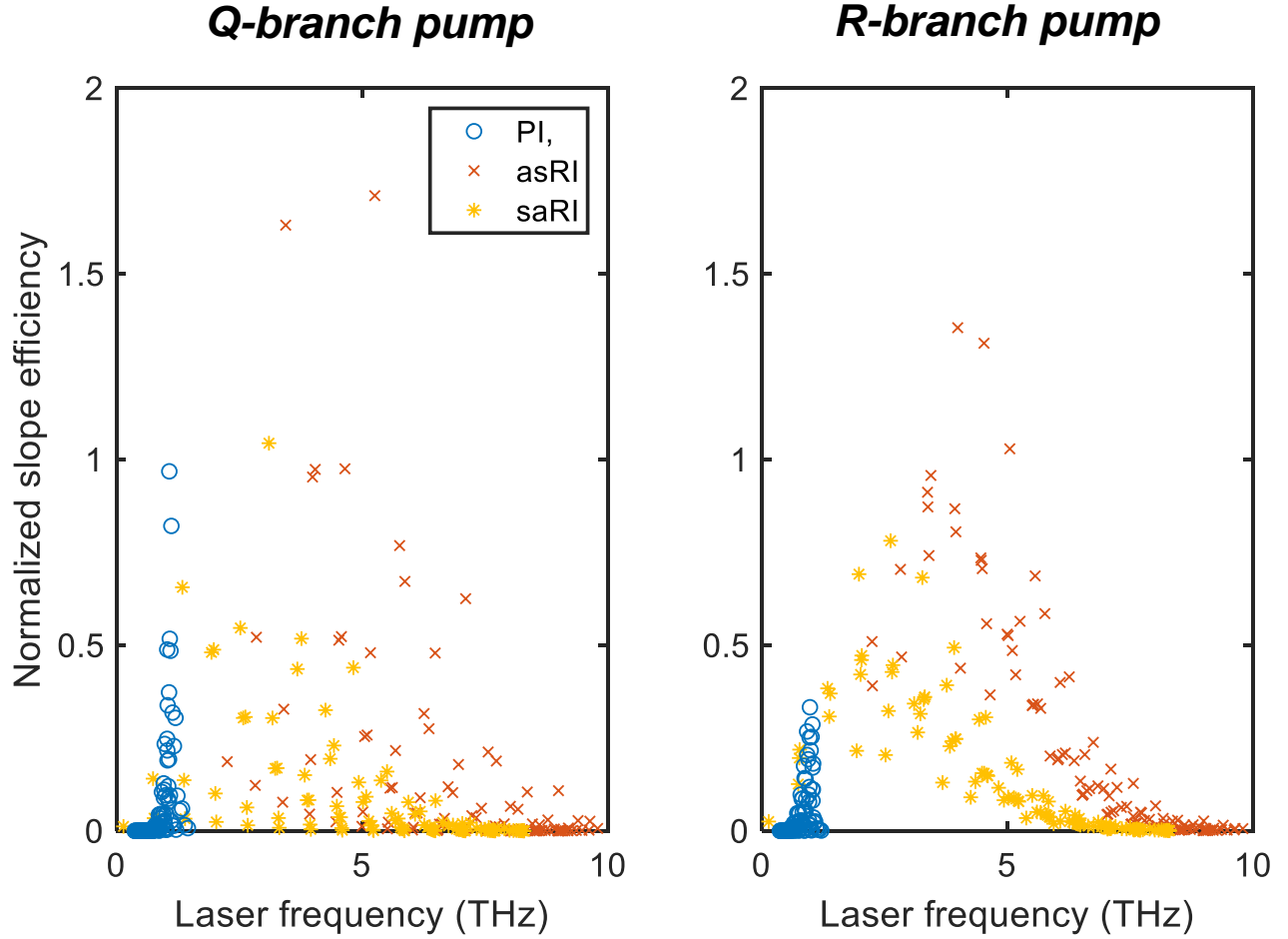


FIG. 3. Normalized slope efficiency of the  $\text{NH}_3$  QPML as function of the transition frequency, using the method of Ref. 4 for a Q-branch or an R-branch pump.

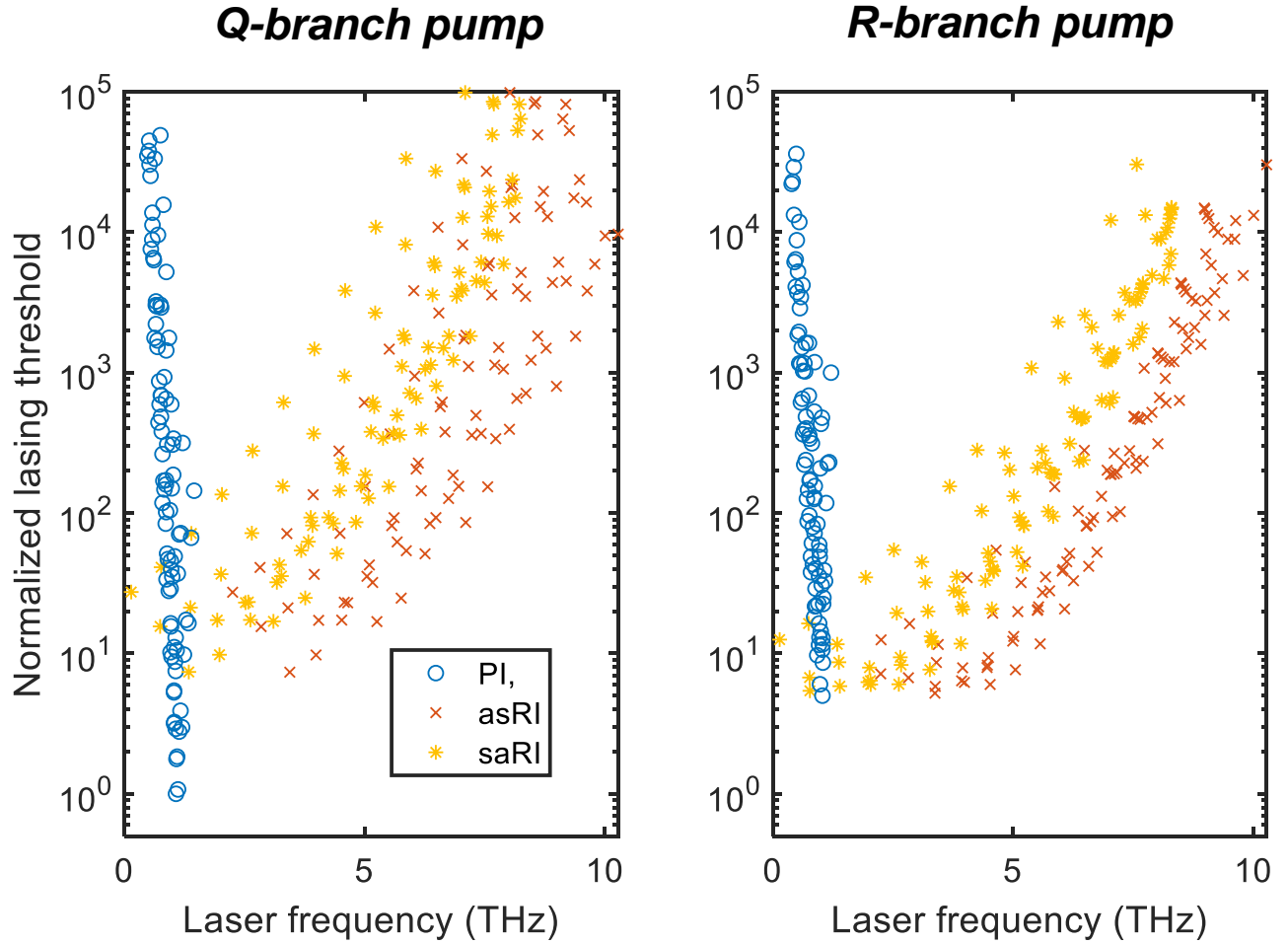


FIG. 4. Normalized lasing threshold of the  $\text{NH}_3$  QPML as function of the transition frequency, using the method of Ref. 4 for a Q-branch or an R-branch pump.

TABLE I. Frequencies of RIas and PI direct lasing and RIa cascaded lasing, as a function of the saR infrared transitions wavenumber

saR pump wavenumber (cm <sup>-1</sup> )	<i>J<sub>L</sub></i>	<i>J<sub>U</sub></i>	<i>K</i>	Lasing frequency direct PI (THz)	Lasing frequency direct RIas (THz)	Lasing frequency PI-cascaded RIa (THz)	Lasing frequency RIas-cascaded RIa (THz)
1007.547	1	2	0	-	2.2445	-	-
1007.540	1	2	1	1.0453	2.2521	0.1401	-
1027.047	2	3	1	1.0141	2.8223	0.7629	0.1401
1027.033	2	3	2	1.0358	2.8453	0.7418	-
1046.405	3	4	0	-	3.3735	-	0.7698
1046.401	3	4	1	0.9738	3.3810	1.3931	0.7629
1046.388	3	4	2	0.9947	3.4036	1.3730	0.7418
1046.375	3	4	3	1.0305	3.4423	1.3388	-
1065.594	4	5	1	0.9257	3.9287	2.0292	1.3931
1065.582	4	5	2	0.9456	3.9507	2.0104	1.3730
1065.568	4	5	3	0.9797	3.9884	1.9781	1.3388
1065.564	4	5	4	1.0294	4.0430	1.9310	-
1084.629	5	6	0	-	4.4589	-	2.0354
1084.623	5	6	1	0.8709	4.4659	2.6694	2.0292
1084.610	5	6	2	0.8897	4.4872	2.6519	2.0104
1084.593	5	6	3	0.9219	4.5236	2.6219	1.9781
1084.584	5	6	4	0.9688	4.5764	2.5782	1.9310
1084.600	5	6	5	1.0323	4.6476	2.5187	-
1103.485	6	7	1	0.8109	4.9936	3.3117	2.6694
1103.469	6	7	2	0.8285	5.0140	3.2957	2.6519
1103.448	6	7	3	0.8586	5.0488	3.2682	2.6219
1103.432	6	7	4	0.9025	5.0993	3.2280	2.5782
1103.436	6	7	5	0.9619	5.1675	3.1733	2.5187
1103.480	6	7	6	1.0394	5.2560	3.1015	-
1122.184	7	8	0	-	5.5061	-	3.3170
1122.177	7	8	1	0.7473	5.5125	3.9542	3.3117
1122.158	7	8	2	0.7636	5.5319	3.9397	3.2957
1122.132	7	8	3	0.7915	5.5650	3.9149	3.2682
1122.107	7	8	4	0.8321	5.6130	3.8785	3.2280
1122.096	7	8	5	0.8871	5.6778	3.8288	3.1733
1122.120	7	8	6	0.9589	5.7618	3.7636	3.1015
1122.205	7	8	7	1.0505	5.8684	3.6796	-
1140.696	8	9	1	0.6816	6.0237	4.5947	3.9542
1140.675	8	9	2	0.6965	6.0420	4.5819	3.9397
1140.643	8	9	3	0.7220	6.0732	4.5597	3.9149
1140.608	8	9	4	0.7592	6.1185	4.5273	3.8785
1140.583	8	9	5	0.8096	6.1796	4.4829	3.8288
1140.584	8	9	6	0.8754	6.2588	4.4245	3.7636
1140.636	8	9	7	0.9596	6.3592	4.3490	3.6796
1140.773	8	9	8	1.0659	6.4848	4.2527	-
1159.050	9	10	0	-	6.5225	-	4.5990
1159.041	9	10	1	0.6152	6.5282	5.2314	4.5947
1159.016	9	10	2	0.6287	6.5453	5.2202	4.5819
1158.979	9	10	3	0.6518	6.5746	5.2008	4.5597
1158.936	9	10	4	0.6855	6.6170	5.1724	4.5273
1158.896	9	10	5	0.7312	6.6742	5.1334	4.4829
1158.875	9	10	6	0.7910	6.7483	5.0818	4.4245
1158.894	9	10	7	0.8675	6.8421	5.0151	4.3490
1158.983	9	10	8	0.9641	6.9596	4.9296	4.2527
1159.184	9	10	9	1.0855	7.1054	4.8207	-
1177.206	10	11	1	0.5495	7.0270	5.8624	5.2314
1177.179	10	11	2	0.5616	7.0430	5.8527	5.2202
1177.138	10	11	3	0.5823	7.0702	5.8361	5.2008
1177.086	10	11	4	0.6125	7.1097	5.8117	5.1724
1177.034	10	11	5	0.6536	7.1629	5.7781	5.1334
1176.992	10	11	6	0.7072	7.2317	5.7335	5.0818
1176.980	10	11	7	0.7760	7.3188	5.6754	5.0151
1177.023	10	11	8	0.8630	7.4278	5.6007	4.9296
1177.158	10	11	9	0.9724	7.5631	5.5052	4.8207
1177.437	10	11	10	1.1096	7.7305	5.3834	-

TABLE II. Frequencies of RI<sub>a</sub> direct lasing and PI and RI<sub>a</sub>s cascaded lasing, as a function of the asR infrared transitions wavenumber

asR pump wavenumber (cm <sup>-1</sup> )	<i>J<sub>L</sub></i>	<i>J<sub>U</sub></i>	<i>K</i>	Lasing frequency direct RI <sub>a</sub> (THz)	Lasing frequency cascaded PI (THz)	Lasing frequency cascaded RI <sub>a</sub> s (THz)
971.882	1	2	1	0.1401	1.0667	-
992.701	2	3	0	0.7698	-	2.2445
992.450	2	3	1	0.7629	1.0453	2.2521
991.691	2	3	2	0.7418	1.0677	-
1013.176	3	4	1	1.3931	1.0141	2.8223
1012.445	3	4	2	1.3730	1.0358	2.8453
1011.204	3	4	3	1.3388	1.0730	-
1034.243	4	5	0	2.0354	-	3.3735
1034.013	4	5	1	2.0292	0.9738	3.3810
1033.316	4	5	2	2.0104	0.9947	3.4036
1032.131	4	5	3	1.9781	1.0305	3.4423
1030.422	4	5	4	1.9310	1.0826	-
1054.912	5	6	1	2.6694	0.9257	3.9287
1054.252	5	6	2	2.6519	0.9456	3.9507
1053.131	5	6	3	2.6219	0.9797	3.9884
1051.512	5	6	4	2.5782	1.0294	4.0430
1049.347	5	6	5	2.5187	1.0966	-
1076.026	6	7	0	3.3170	-	4.4589
1075.821	6	7	1	3.3117	0.8709	4.4659
1075.202	6	7	2	3.2957	0.8897	4.4872
1074.148	6	7	3	3.2682	0.9219	4.5236
1072.628	6	7	4	3.2280	0.9688	4.5764
1070.592	6	7	5	3.1733	1.0323	4.6476
1067.975	6	7	6	3.1015	1.1151	-
1096.686	7	8	1	3.9542	0.8109	4.9936
1096.110	7	8	2	3.9397	0.8285	5.0140
1095.128	7	8	3	3.9149	0.8586	5.0488
1093.711	7	8	4	3.8785	0.9025	5.0993
1091.813	7	8	5	3.8288	0.9619	5.1675
1089.371	7	8	6	3.7636	1.0394	5.2560
1086.305	7	8	7	3.6796	1.1382	-
1117.628	8	9	0	4.5990	-	5.5061
1117.453	8	9	1	4.5947	0.7473	5.5125
1116.920	8	9	2	4.5819	0.7636	5.5319
1116.014	8	9	3	4.5597	0.7915	5.5650
1114.705	8	9	4	4.5273	0.8321	5.6130
1112.950	8	9	5	4.4829	0.8871	5.6778
1110.692	8	9	6	4.4245	0.9589	5.7618
1107.852	8	9	7	4.3490	1.0505	5.8684
1104.334	8	9	8	4.2527	1.1662	-
1138.066	9	10	1	5.2314	0.6816	6.0237
1137.580	9	10	2	5.2202	0.6965	6.0420
1136.751	9	10	3	5.2008	0.7220	6.0732
1135.552	9	10	4	5.1724	0.7592	6.1185
1133.945	9	10	5	5.1334	0.8096	6.1796
1131.873	9	10	6	5.0818	0.8754	6.2588
1129.267	9	10	7	5.0151	0.9596	6.3592
1126.034	9	10	8	4.9296	1.0659	6.4848
1122.058	9	10	9	4.8207	1.1992	-
1158.622	10	11	0	5.8655	-	6.5225
1158.476	10	11	1	5.8624	0.6152	6.5282
1158.035	10	11	2	5.8527	0.6287	6.5453
1157.284	10	11	3	5.8361	0.6518	6.5746
1156.197	10	11	4	5.8117	0.6855	6.6170
1154.739	10	11	5	5.7781	0.7312	6.6742
1152.857	10	11	6	5.7335	0.7910	6.7483
1150.486	10	11	7	5.6754	0.8675	6.8421
1147.542	10	11	8	5.6007	0.9641	6.9596
1143.915	10	11	9	5.5052	1.0855	7.1054
1139.471	10	11	10	5.3834	1.2375	-

TABLE III. Frequencies of RIas and PI direct lasing and RIa cascaded lasing, as a function of the saQ infrared transitions wavenumber

saQ pump wavenumber (cm <sup>-1</sup> )	<i>J<sub>L</sub></i>	<i>J<sub>U</sub></i>	<i>K</i>	Lasing frequency direct PI (THz)	Lasing frequency direct RIas (THz)	Lasing frequency PI-cascaded RIa (THz)	Lasing frequency RIas-cascaded RIa (THz)
967.998	1	1	1	1.0667	-	-	-
967.775	2	2	1	1.0453	2.2521	0.1401	-
967.738	2	2	2	1.0677	-	-	-
967.449	3	3	1	1.0141	2.8223	0.7629	0.1401
967.407	3	3	2	1.0358	2.8453	0.7418	-
967.344	3	3	3	1.0730	-	-	-
967.031	4	4	1	0.9738	3.3810	1.3931	0.7629
966.981	4	4	2	0.9947	3.4036	1.3730	0.7418
966.905	4	4	3	1.0305	3.4423	1.3388	-
966.815	4	4	4	1.0826	-	-	-
966.532	5	5	1	0.9257	3.9287	2.0292	1.3931
966.474	5	5	2	0.9456	3.9507	2.0104	1.3730
966.382	5	5	3	0.9797	3.9884	1.9781	1.3388
966.269	5	5	4	1.0294	4.0430	1.9310	-
966.151	5	5	5	1.0966	-	-	-
965.967	6	6	1	0.8709	4.4659	2.6694	2.0292
965.899	6	6	2	0.8897	4.4872	2.6519	2.0104
965.791	6	6	3	0.9219	4.5236	2.6219	1.9781
965.653	6	6	4	0.9688	4.5764	2.5782	1.9310
965.500	6	6	5	1.0323	4.6476	2.5187	-
965.354	6	6	6	1.1151	-	-	-
965.351	7	7	1	0.8109	4.9936	3.3117	2.6694
965.272	7	7	2	0.8285	5.0140	3.2957	2.6519
965.146	7	7	3	0.8586	5.0488	3.2682	2.6219
964.981	7	7	4	0.9025	5.0993	3.2280	2.5782
964.791	7	7	5	0.9619	5.1675	3.1733	2.5187
964.597	7	7	6	1.0394	5.2560	3.1015	-
964.424	7	7	7	1.1382	-	-	-
964.697	8	8	1	0.7473	5.5125	3.9542	3.3117
964.608	8	8	2	0.7636	5.5319	3.9397	3.2957
964.463	8	8	3	0.7915	5.5650	3.9149	3.2682
964.271	8	8	4	0.8321	5.6130	3.8785	3.2280
964.044	8	8	5	0.8871	5.6778	3.8288	3.1733
963.799	8	8	6	0.9589	5.7618	3.7636	3.1015
963.560	8	8	7	1.0505	5.8684	3.6796	-
963.363	8	8	8	1.1662	-	-	-
964.020	9	9	1	0.6816	6.0237	4.5990	3.9542
963.920	9	9	2	0.6965	6.0420	4.5947	3.9397
963.758	9	9	3	0.7220	6.0732	4.5819	3.9149
963.539	9	9	4	0.7592	6.1185	4.5597	3.8785
963.274	9	9	5	0.8096	6.1796	4.5273	3.8288
962.979	9	9	6	0.8754	6.2588	4.4829	3.7636
962.674	9	9	7	0.9596	6.3592	4.4245	3.6796
962.391	9	9	8	1.0659	6.4848	4.3490	-
962.172	9	9	9	1.1992	-	4.2527	-
963.330	10	10	1	0.6152	6.5282	5.2314	4.5990
963.221	10	10	2	0.6287	6.5453	5.2202	4.5947
963.042	10	10	3	0.6518	6.5746	5.2008	4.5819
962.798	10	10	4	0.6855	6.6170	5.1724	4.5597
962.498	10	10	5	0.7312	6.6742	5.1334	4.5273
962.154	10	10	6	0.7910	6.7483	5.0818	4.4829
961.785	10	10	7	0.8675	6.8421	5.0151	4.4245
961.418	10	10	8	0.9641	6.9596	4.9296	4.3490
961.090	10	10	9	1.0855	7.1054	4.8207	4.2527
960.853	10	10	10	1.2375	-	-	-

TABLE IV. Frequencies of RI<sub>sa</sub> direct lasing and PI and RI<sub>as</sub> cascaded lasing, as a function of the asQ infrared transitions wavenumber

asQ pump wavenumber (cm <sup>-1</sup> )	<i>J<sub>L</sub></i>	<i>J<sub>U</sub></i>	<i>K</i>	Lasing frequency direct RI <sub>sa</sub> (THz)	Lasing frequency cascaded PI (THz)	Lasing frequency cascaded RI <sub>as</sub> (THz)
932.136	2	2	1	0.1401	1.0667	-
932.881	3	3	1	0.7629	1.0453	2.2521
932.094	3	3	2	0.7418	1.0677	-
933.843	4	4	1	1.3931	1.0141	2.8223
933.076	4	4	2	1.3730	1.0358	2.8453
931.774	4	4	3	1.3388	1.0730	-
934.994	5	5	1	2.0292	0.9738	3.3810
934.252	5	5	2	2.0104	0.9947	3.4036
932.992	5	5	3	1.9781	1.0305	3.4423
931.177	5	5	4	1.9310	1.0826	-
936.304	6	6	1	2.6694	0.9257	3.9287
935.591	6	6	2	2.6519	0.9456	3.9507
934.380	6	6	3	2.6219	0.9797	3.9884
932.636	6	6	4	2.5782	1.0294	4.0430
930.307	6	6	5	2.5187	1.0966	-
937.739	7	7	1	3.3117	0.8709	4.4659
937.058	7	7	2	3.2957	0.8897	4.4872
935.902	7	7	3	3.2682	0.9219	4.5236
934.236	7	7	4	3.2280	0.9688	4.5764
932.012	7	7	5	3.1733	1.0323	4.6476
929.162	7	7	6	3.1015	1.1151	-
939.260	8	8	1	3.9542	0.8109	4.9936
938.614	8	8	2	3.9397	0.8285	5.0140
937.517	8	8	3	3.9149	0.8586	5.0488
935.937	8	8	4	3.8785	0.9025	5.0993
933.827	8	8	5	3.8288	0.9619	5.1675
931.123	8	8	6	3.7636	1.0394	5.2560
927.743	8	8	7	3.6796	1.1382	-
940.830	9	9	1	4.5947	0.7473	5.5125
940.221	9	9	2	4.5819	0.7636	5.5319
939.187	9	9	3	4.5597	0.7915	5.5650
937.698	9	9	4	4.5273	0.8321	5.6130
935.709	9	9	5	4.4829	0.8871	5.6778
933.160	9	9	6	4.4245	0.9589	5.7618
929.973	9	9	7	4.3490	1.0505	5.8684
926.047	9	9	8	4.2527	1.1662	-
942.408	10	10	1	5.2314	0.6816	6.0237
941.838	10	10	2	5.2202	0.6965	6.0420
940.870	10	10	3	5.2008	0.7220	6.0732
939.475	10	10	4	5.1724	0.7592	6.1185
937.612	10	10	5	5.1334	0.8096	6.1796
935.225	10	10	6	5.0818	0.8754	6.2588
932.240	10	10	7	5.0151	0.9596	6.3592
928.562	10	10	8	4.9296	1.0659	6.4848
924.073	10	10	9	4.8207	1.1992	-